Acylation of the RTX toxin MbxA stimulates host membrane disruption through a specific interaction with cholesterol

Feby Mariam Chacko, Sarah Michelle Ganz, Anne Pfitzer-Bilsing, Sebastian Hänsch, Philipp Westhoff, Stefanie Weidtkamp-Peters, Sander H.J. Smits, Marten Exterkate, Lutz Schmitt

Article - Version of Record

BBA - Biomembranes 1868 (2026) 184487

Contents lists available at ScienceDirect

BBA - Biomembranes

journal homepage: www.elsevier.com/locate/bbamem

Research paper

Acylation of the RTX toxin MbxA stimulates host membrane disruption through a specific interaction with cholesterol

Feby Mariam Chacko [a], Sarah Michelle Ganz [a], Anne Pfitzer-Bilsing [a], Sebastian Hänsch [b], Philipp Westhoff [c], Stefanie Weidtkamp-Peters [b], Sander H.J. Smits [a,d], Marten Exterkate [e], Lutz Schmitt [a,*]

[a] Institute of Biochemistry, Heinrich-Heine-University Düsseldorf, Universitätsstraße 1, 40225, Düsseldorf, Germany
[b] Center for Advanced Imaging, Heinrich Heine University Düsseldorf, Universitätsstraße 1, 40225, Düsseldorf, Germany
[c] Metabolomics and Metabolism Laboratory, Cluster of Excellence for Plant Sciences (CEPLAS), Heinrich Heine University Düsseldorf, Germany
[d] Center for Structural Studies, Heinrich Heine University Düsseldorf, Universitätsstraße 1, 40225, Düsseldorf, Germany
[e] Membrane Biogenesis and Lipidomics Group, Heinrich Heine University Düsseldorf, Universitätsstraße 1, 40225, Düsseldorf, Germany

ARTICLE INFO

Keywords:
RTX toxins
MbxA
Acylation
Cholesterol
Lipid composition
Membrane disruption
Membrane fluidity

ABSTRACT

RTX toxins (Repeat in ToXins) are pore-forming toxins secreted by gram-negative bacteria. They are known for their ability to disrupt host cell membranes, among which various human cells. The acylation of specific lysine residues in these toxins is crucial for their hemolytic activity, but the precise mechanisms underlying this enhancement remain unclear. By comparing the lytic activities of acylated MbxA and its non-acylated form, we explored the role of acylation in the pore-forming behavior of this RTX toxin. Our findings demonstrate that acylation specific interactions of MbxA with cholesterol promote membrane disruption, both *in vitro* and in living cells. More specifically, acylation is not necessary for initial membrane binding, but markedly enhances pore formation. Overall, our results provide detailed insights into the molecular determinants that regulate MbxA toxin activity. We highlight a complex interplay between lipid composition (sterols), acylation, and membrane disruption, thereby advancing our general understanding of RTX toxin pathogenesis.

1. Introduction

RTX (repeats-in-toxin) toxins are a family of exoproteins secreted by Gram-negative bacteria through a Type-1 secretion system (T1SS) [1]. Many bacteria utilize these pore-forming RTX toxins [2] as virulence factors during infection. For instance, the uropathogenic *Escherichia coli* hemolysin A (HlyA) is an RTX toxin linked to urinary tract infections, one of the most common bacterial infections worldwide [3]. Another example is the Adenylate Cyclase Toxin from *Bordetella pertussis*. This bacteria targets the human respiratory tract and causes whooping cough, a highly contagious and recurring disease [4]. Furthermore, the oral bacterium *Aggregatibacter actinomycetemcomitans* (known to cause localized aggressive periodontitis and endocarditis), produces an RTX protein called leukotoxin A (LtxA), which is lethal to human immune cells [5].

RTX proteins are distinguished by the presence of calcium-binding glycine-rich nonapeptide repeats (GGxGxDxUx; where x represents any amino acid and U indicates a large hydrophobic amino acid) located in the C-terminal part of the protein [6]. HlyA serves as the prototype of the RTX toxin family research. In the cytoplasm of *E. coli*, the translated HlyA remains unfolded and inactive prior to secretion [7,8]. It becomes active through post-translational acylation at two lysine residues, K564 and K690, which is catalyzed by the acyl transferase HlyC [9]. These acyl modifications are essential for hemolytic activity and represent a crucial activation step that distinguishes functional RTX toxins from their inactive precursors. The acylated HlyA is then secreted *via* the T1SS, composed of the ABC transporter HlyB (the inner membrane protein), HlyD (the membrane fusion protein), and TolC (the outer membrane protein) [10]. Once the entire HlyA protein is outside the cell, it fully folds through binding of calcium and becomes active, ready to form pores in various types of cells.

Secreted RTX toxins generally exhibit a broad range of host cell specificity [6,11]. Many RTX toxins have been shown to interact with specific β_2 integrin receptors of certain host cells, such as Jurkat cells

* Corresponding author.
E-mail address: Lutz.Schmitt@hhu.de (L. Schmitt).

https://doi.org/10.1016/j.bbamem.2025.184487
Received 24 July 2025; Received in revised form 24 October 2025; Accepted 23 November 2025
Available online 27 November 2025

(human T-lymphocyte cells) [3,12–21]. However, not all RTX toxins rely on β_2 integrin receptors to interact with host cell membranes. For instance, the RTX toxin RtxA from *Kingella kingae* does not engage with β_2 integrin receptors at all [22]. Likewise, several RTX toxins induce cytotoxicity in red blood cells that lack β_2 integrin receptors [23,24]. Moreover, pore-forming and lytic properties of RTX toxins have been demonstrated in various artificial membranes [25,26]. Overall, these findings suggest a β_2 integrin receptor-independent mechanism for RTX toxin interaction with host cell membranes. Indeed, several RTX toxins have been associated with non-protein structures on host cell membranes, such as the carbohydrate chains of glycophorins, gangliosides, and cholesterol, further supporting the idea of a receptor-independent interaction pathway [4,22,27–36]. However, the precise mechanism by which they facilitate RTX toxin pore formation remains poorly understood.

Moraxella bovis is an intracellular parasite that inhabits mucous membranes and causes the ocular disease infectious bovine keratoconjunctivitis in cattle. MbxA is an uncharacterized RTX toxin produced by *M. bovis*. In this study, we employed an established heterologous system to secrete both the acylated, active form of MbxA and the non-acylated, inactive form using the *E. coli* T1SS [37]. MbxA shares 42 % sequence identity with HlyA, and alternative to the *hly* operon (*hlyB, hlyD, and tolc*), the RTX operon of *M. bovis* contains all the genes required for activation (*mbxC*) and secretion (*mbxB*, *mbxD*, and *tolC*) of an RTX toxin [37–44], which helped in the successful heterologous secretion of MbxA using *E. coli* T1SS.

Our previous work demonstrated that MbxA induces cytotoxicity in a wide variety of cells, including sheep red blood cells, suggesting that MbxA also exhibits activity independent of β_2 integrin receptors [37]. Here, we further explore the mechanisms underlying MbxA-mediated cytotoxicity, in which we specifically focus on the role of the lipid membrane. By combining *in vitro* and *in vivo* approaches, we reveal a prominent role for cholesterol in the pore-forming activity of MbxA, which is acylation-dependent.

2. Results

2.1. A liposome leakage assay to understand the lipid dependency in the lytic activity of acylated MbxA and non-acylated proMbxA

To examine the β_2 integrin receptor-independent pore-forming activity of MbxA, we conducted a commonly used liposome leakage assay, based on the fluorophore 8-Aminonaphthalene-1,3,6-Trisulphonic acid (ANTS) and its quencher p-Xylene-Bis-Pyridinium Bromide (DPX) (Fig. 1a). The ANTS/DPX system relies on concentration-dependent quenching: when encapsulated together at high concentration within liposomes, DPX quenches ANTS fluorescence. Pore formation allows leakage and dilution of the contents into the bulk solution, spatially separating ANTS from DPX and resulting in fluorescence dequenching proportional to the degree of membrane disruption. In the liposome leakage assay, after establishing baseline fluorescence, 100 nM of either acylated MbxA or non-acylated proMbxA was added to the liposomes, thereby initiating possible pore formation/leakage. After reaching a stable plateau, 0.5 % Triton X-100 was introduced, dissolving all liposomes. As a consequence, the measured fluorescence represents 100 % content release (Fig. 1b).

2.2. Increased lytic activity of MbxA and proMbxA for liposomes composed of unsaturated fatty acids and negatively charged lipid headgroups

To investigate the lipid dependency of pore formation by MbxA and proMbxA, we assessed the lytic activity of the proteins on a series of liposomes with varying lipid compositions based on either the saturation of their lipid tails or the charge of the headgroup. Focusing on the acyl chains, three different lipid species were chosen: di-palmitoyl phosphatidylcholine (DPPC), which has two saturated acyl chains, palmitoyl-oleoyl phosphatidylcholine (POPC) containing one unsaturated acyl chain, and di-oleoyl phosphatidylcholine (DOPC), which consists of two unsaturated acyl chains (lipid saturation in the order DPPC>POPC>DOPC). Both MbxA and proMbxA exhibited a higher pore-forming efficiency in the presence of the highly unsaturated DOPC liposomes, while only limited pore formation was observed for the fully saturated DPPC liposomes (Fig. 2a) as evident by the lower fluorescence increase after protein addition for DPPC liposomes. Notably, MbxA demonstrated a specific activity compared to proMbxA, most pronounced for POPC liposomes, illustrating that the acyl moieties of the protein affect the lytic activity under specific membrane conditions. Subsequently, the lytic activity of MbxA and proMbxA was tested in the presence of different head groups, differing in their overall charge. While POPC possesses a net neutral charge, palmitoyl-oleoyl phosphatidylserine (POPS) has a net negative charge (lipid headgroup charge: POPS>POPC:POPS 1:1 > POPC). Both MbxA and proMbxA exhibited increased lytic activity toward the negatively charged liposomes

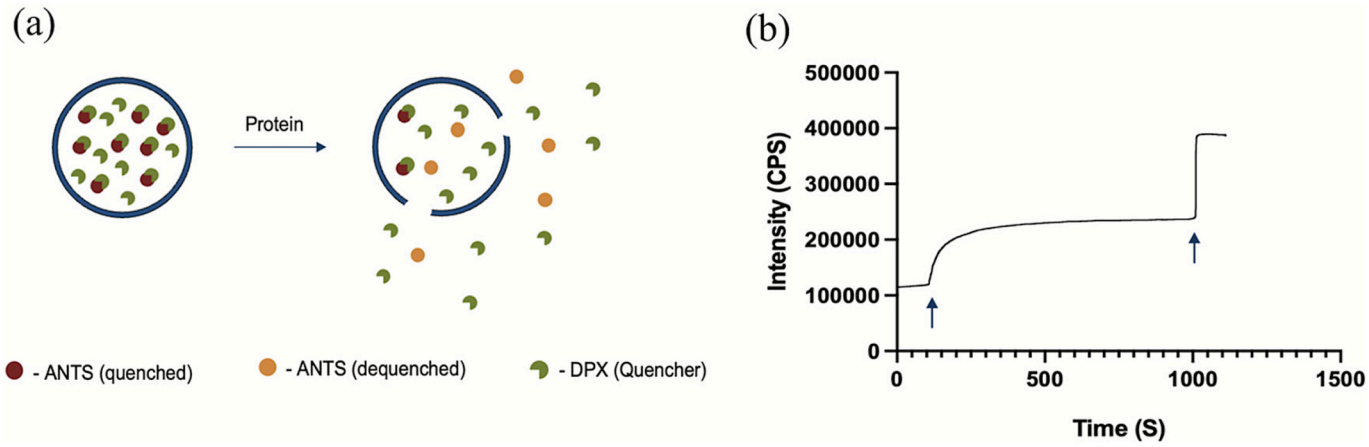

Fig. 1. (a) ANTS (8-Aminonaphthalene-1,3,6-Trisulphonic acid) is a fluorophore that is quenched by DPX (p-Xylene-Bis-Pyridinium Bromide) when both are co-encapsulated at high concentrations within liposomes. Upon pore formation by MbxA or proMbxA, the liposomal contents leak out into the surrounding buffer, where dilution spatially separates ANTS from DPX, relieving the quenching effect and resulting in increased fluorescence intensity. The magnitude of fluorescence increase is proportional to the extent of liposomal leakage. (b) Fluorescence measurement of DOPC liposomes encapsulated with ANTS/DPX prepared from 12 μM DOPC. After 100 s, 100 nM MbxA is added (first arrow). Once a plateau is reached, 0.5 % Triton X-100 was added (second arrow), resulting in the complete release of the liposomal content.

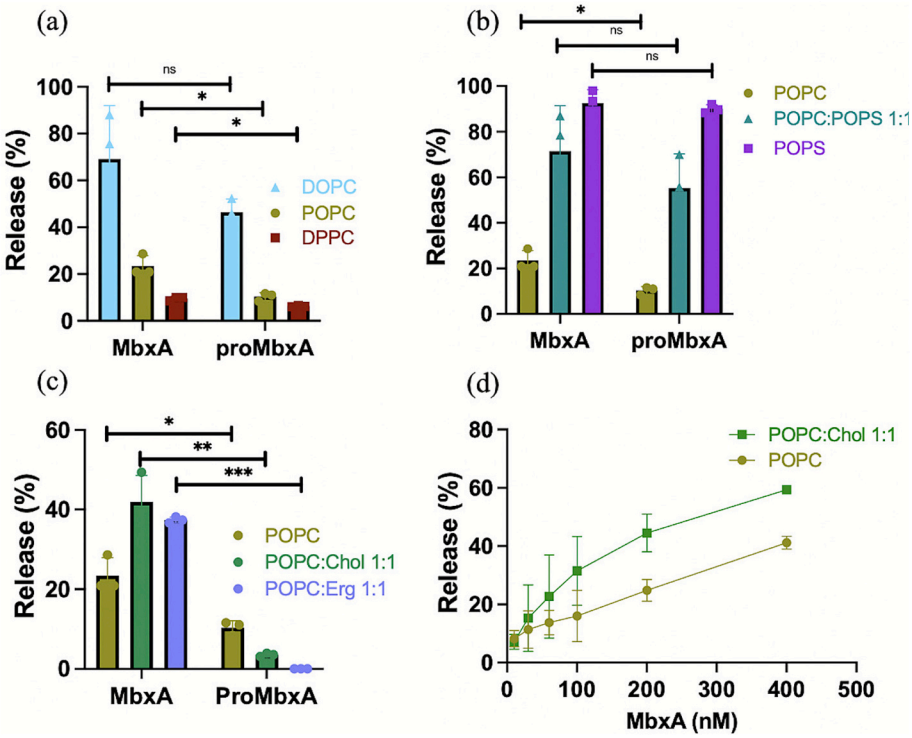

Fig. 2. The percentage release of liposomal content by the lytic activity of MbxA and proMbxA on different sets of liposomes. Lytic activity of MbxA and proMbxA on liposomes based on (a) the acyl chain saturation of the lipid chain, (b) the charge of the lipid head group, and (c) cholesterol and ergosterol incorporation into the liposomes. 100 nM (pro)MbxA was added to 12 uM liposomes (final lipid concentration), and fluorescence release was measured for 15 min. (d) Percentage release of liposomal content when different concentrations of MbxA were incubated with 12 uM POPC and POPC:Chol 1:1 liposomes. Statistical analysis was performed using an unpaired *t*-test, and for each liposomal lipid composition the maximal release values between MbxA and proMbxA were checked to see if they were biologically not significant (ns) or significant (* if $p < 0.05$, ** if $p < 0.01$; *** if $p < 0.001$). Data shown represent biological replicates ($n = 3$).

(Fig. 2b). Moreover, the difference in lytic activity between MbxA and proMbxA seems to diminish upon increase of POPS, indicating no specific interaction between the acyl-chain moieties of the protein and the lipid headgroup.

2.3. MbxA exhibits specific lytic activity toward cholesterol-containing liposomes, while proMbxA does not

Given that cholesterol is present in mammalian cell membranes but absent in bacterial cell membranes, we assessed whether MbxA and proMbxA exhibit specific lytic activity against cholesterol-containing membranes. Although the highest lytic activity was shown in the presence of POPS liposomes, anionic lipids are predominantly found in the inner leaflet of mammalian plasma membranes [45]. For this reason, we continued with POPC liposomes as they are most representative of the outer leaflet. When cholesterol was added to POPC liposomes at a 1:1 ratio, a 2.5-fold increase in liposome leakage was observed for MbxA compared to POPC liposomes, whereas proMbxA showed no such increase (Fig. 2c).

A specific role of the acylation moieties of MbxA in the lytic activity of the protein was already observed for POPC liposomes, but seems to be further enhanced in the presence of cholesterol. To further elucidate this phenomenon, we tested the lytic activity of POPC *vs.* POPC:Chol liposomes at varying MbxA concentrations (10 nM, 30 nM, 60 nM, 100 nM, 200 nM, and 400 nM) (Fig. 2d, Supplementary fig. 2a,b). For both sets of liposomes, we observed a linear increase in the release of liposomal content, but the POPC:Chol liposomes exhibit an overall higher release, thereby confirming the stimulating effect of cholesterol on the lytic activity of MbxA.

Furthermore, we examined the lytic activity of MbxA and proMbxA in the presence of sterols other than cholesterol by incorporating ergosterol into POPC liposomes (POPC:Ergosterol 1:1). Remarkably, similar to cholesterol, ergosterol enhanced the leakage of liposomal content when incubated with MbxA, although it did not have the same effect on proMbxA (Fig. 2c).

Given that gangliosides have been reported as receptors for other RTX toxins [29,30,34], we further investigated the effect of gangliosides on the lytic activity of MbxA and proMbxA. However, POPC liposomes containing 30 % GM1 gangliosides did not induce any significant lytic activity for either MbxA or proMbxA; in fact, the lytic activity of MbxA decreased by approximately 5 % compared to that observed with POPC liposomes (Supplementary fig. 2c).

2.4. MbxA, but not proMbxA, causes rupture of POPC:Chol GUVs

To visualize the different leakage effects of MbxA *vs.* proMbxA on POPC:Chol liposomes, we prepared Giant Unilamellar Vesicles (GUVs), incubated them with 100 nM of either MbxA or proMbxA and analyzed them by microscope (Evos M5000 imaging system) over time. Upon incubation with MbxA, noticeable changes in the shape of the GUVs were observed within 30 s (Fig. 3b), but they returned to their normal round shapes within 3 min, shown with colored arrow marks (Fig. 3c). Ultimately, after 10 min, the incubation with MbxA resulted in complete destabilization of the GUVs (Fig. 3d). In contrast, the incubation of 100 nM proMbxA with GUVs did not induce any visible disturbances in the GUV architecture, and they remained stable for 30 min (Fig. 3f to j).

2.5. Flotation assay reveals that acyl chains are not essential for toxin binding to the membrane

Previous experiments (Fig. 2c) indicated that the acyl chains play a crucial role in the lytic activity of the protein within cholesterol-containing membranes. To assess the importance of the acyl chains in the binding of the protein to these membranes, we conducted a flotation

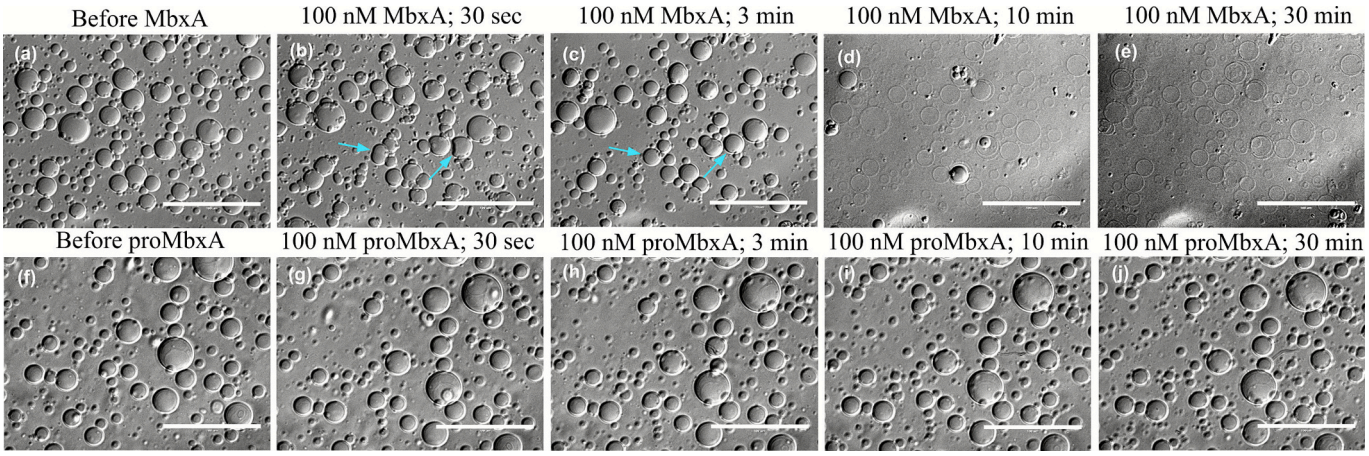

Fig. 3. POPC:Chol 1:1 Giant Unilamellar Vesicles (GUVs) (a) before treatment with MbxA, (b) 30 s (c) 3 min (d) 10 min and (e) 30 min after incubating with 100 nM MbxA, (f) before treatment with proMbxA, (g) 30 s (h) 3 min (i) 10 min and (j) 30 min after incubating with 100 nM proMbxA. Change in GUV shape upon MbxA incubation and its return back to the original shape is shown with colored arrow marks (b&c). The data shown are representative of two biological replicates. Scale bar: 100 μm.

assay using MbxA and proMbxA. In this assay, we established a sucrose gradient ranging from 30 % at the bottom to 0 % at the top. Initially, liposomes incubated with the proteins reside in the bottom fraction. Following ultracentrifugation, the buoyancy of the liposomes causes them to float to the top fraction. If the protein successfully binds to the liposomes, the liposome-bound proteins will also float to the top fraction alongside the liposomes and can be detected *via* SDS-PAGE (Fig. 4a).

The flotation assay using POPC:Chol liposomes and MbxA demonstrated the presence of MbxA in all three fractions: bottom, middle, and top (Fig. 4b). Although, most of the protein was found in the bottom fraction, probably aggregated protein, some protein was detected in the middle and top fraction, indicating liposomal binding. Given the definition of the volume for each fraction, it is expected to observe some protein crossover in the middle fraction from the top fraction. Importantly, the control experiment, which included only MbxA protein without any liposomes, revealed no protein in the top and middle fractions (Fig. 4b). Similarly, the flotation assay with POPC:Chol liposomes and proMbxA indicated that proMbxA also binds to these liposomes (Fig. 4c). Please note that potential liposomal rupture by MbxA inhibits the flotation ability of those liposomes, meaning that the level of observed MbxA in the top fraction could be higher. Nevertheless, the presence of ProMbxA in the top fraction clearly indicates that the acyl chains are not essential for the protein its binding to the membrane.

2.6. *Sterol-induced membrane packing facilitates the insertion of acylated MbxA*

To further elucidate the differences in lytic activity observed between MbxA and proMbxA, we examined the physical properties of membranes containing a variety of lipid compositions. We specifically focused on the fluidity and packing of the membrane, which can be measured by integrating the fluorescent dye Laurdan [46,47]. Membrane fluidity was assessed by measuring the anisotropy, while membrane packing can be evaluated through general polarization (GP) measurements derived from the Laurdan emission spectrum across different lipid compositions (Sup. Fig. 2d). When a sterol such as cholesterol or ergosterol is incorporated into a membrane in a liquid-disordered state ($T > T_m$; T: working temperature, T_m: melting

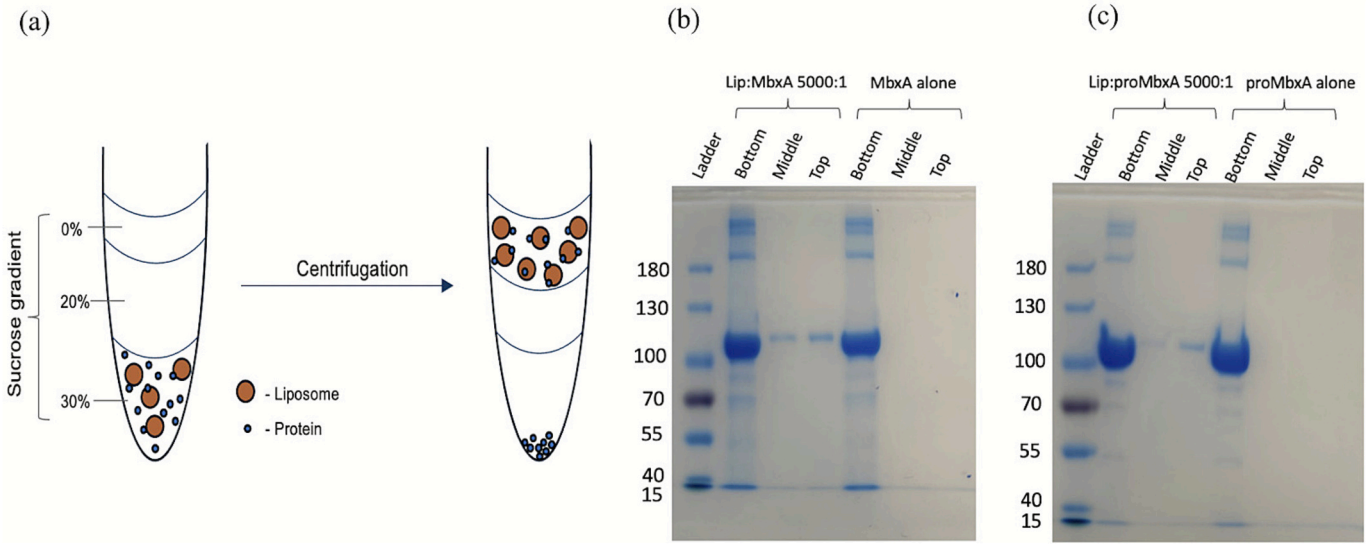

Fig. 4. (a) Schematic representation of the flotation assay. (b) Flotation assay with POPC: Chol 1:1 liposome and MbxA (Lipid: MbxA in 5000:1 ratio). (c) Flotation assay with POPC: Chol 1:1 liposome and proMbxA (Lipid: proMbxA in 5000:1 ratio). Gels are stained using Coomassie brilliant blue. The data shown are representative of two biological replicates. (For interpretation of the references to colour in this figure legend, the reader is referred to the web version of this article.)

temperature), it leads to closer packing of the membrane, resulting in a liquid-ordered state (Fig. 5a). Conversely, when a sterol is integrated into a membrane in a gel phase ($T < T_m$), it results in looser packing of the membrane, also yielding a liquid-ordered state (Fig. 5a).

Anisotropy measurements indicate a similar degree of membrane fluidity for DOPC and POPC liposomes, while DPPC exhibits reduced fluidity (Fig. 5b). This is in accordance with previous observations [48], and indicates that the earlier observed difference in lytic activity between MbxA and proMbxA on POPC membranes (Fig. 2a) is not a consequence of altered membrane fluidity. Concurrently, GP measurements reveal membrane packing in the order of DOPC < POPC < DPPC (Fig. 5c), which does align with the lytic activity of MbxA, observed in

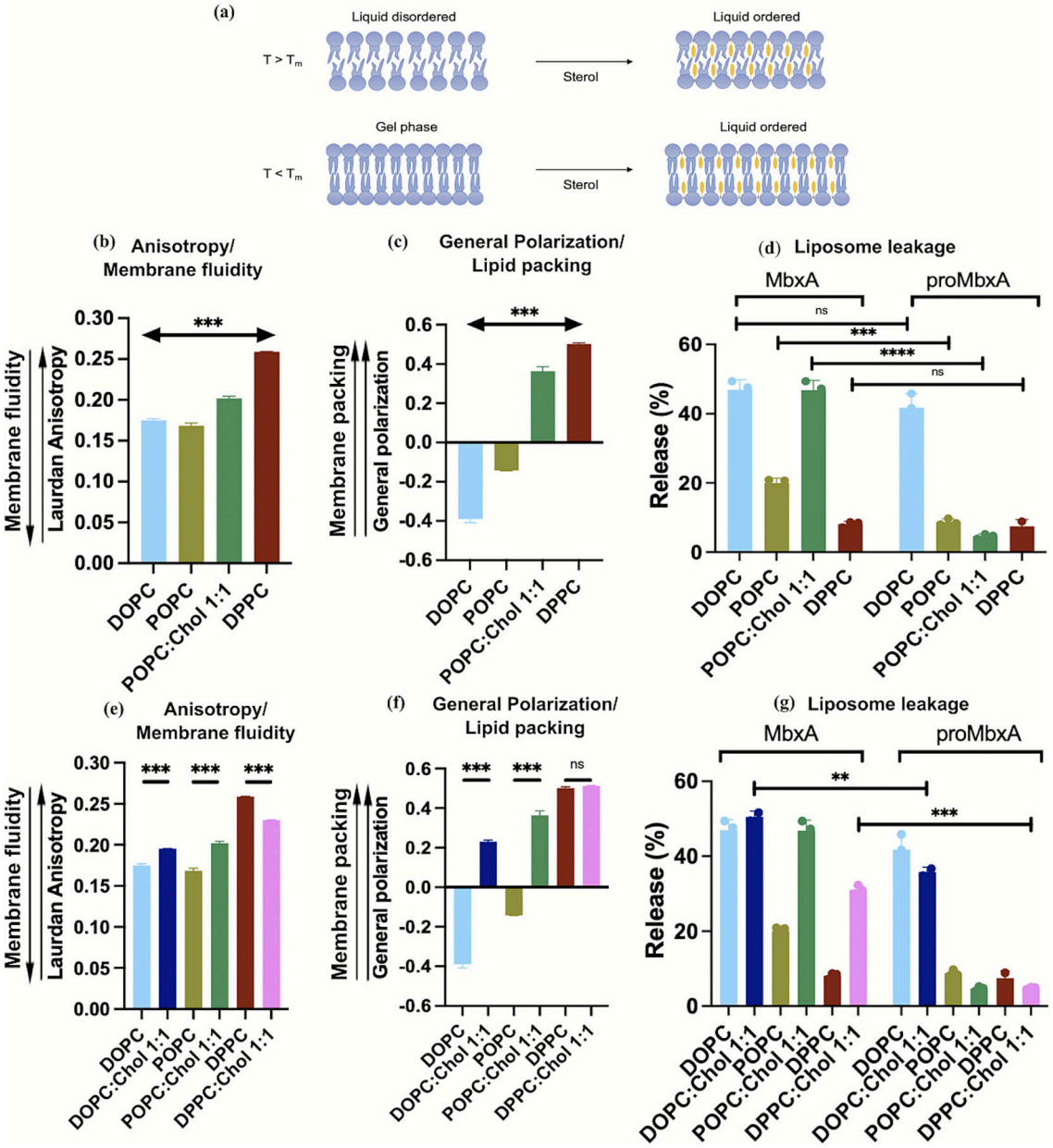

Fig. 5. (a) Theory of lipid packing when sterol is introduced into a membrane in the liquid-disordered state and in the gel phase. (b, e) Anisotropy values of liposomes of different lipid compositions are calculated using the equation $r = (I_{vv} - GI_{vh})/(I_{vv} + 2GI_{vh})$ where I is the fluorescence intensity; v and h are vertical and horizontal settings for the excitation and emission polarizers, respectively; G is the instrumental correction factor provided by the instrument for each instrument (further details are mentioned in the materials and methods section). A higher anisotropy measurement indicates less fluidic membranes and a lower anisotropy measurement indicates highly fluidic membranes. (c, f) General Polarization (GP) values calculated from the Laurdan emission spectrum using the equation $(I_{435} - I_{500})/(I_{435} + I_{500})$, where I is the fluorescence intensity at the respective wavelengths mentioned. A higher GP value (more positive) indicates more closely packed membranes and a lower GP value (more negative) indicates loosely packed membranes. (d, g) Liposome leakage assay of MbxA and proMbxA on liposomes of different lipid compositions. (d) is a combined data of Fig. 2a and c. All the measurements are performed at 20 °C. Lipid compositions with colour codes: DOPC (cyan), DOPC:Chol 1:1 (blue), POPC (light green), POPC:Chol 1:1 (dark green), DPPC (brown), DPPC:Chol 1:1 (magenta). Statistical analysis for Anisotropy and GP measurements was performed using a one-way ANOVA test for overall significance between different lipids, and Turkey's post hoc test for pairwise significance. The significance of maximal liposomal release values between MbxA and proMbxA of DOPC:Chol and DPPC:Chol was checked using an unpaired t-test. ns (not significant) if $p > 0.05$; * if $p < 0.05$, ** if $p < 0.01$; *** if $p < 0.001$. One-way ANOVA test for Anisotropy: $p = 3.80 \times 10^{-8}$(significant); for GP: $p = 2.67 \times 10^{-7}$(significant). The data shown are representative of two biological replicates. (For interpretation of the references to colour in this figure legend, the reader is referred to the web version of this article.)

the order of DOPC > POPC > DPPC (Fig. 2a). In other words, MbxA demonstrates greater lytic activity when the packing of the membrane decreases.

Next, the effect of cholesterol on membrane packing and fluidity was examined. Since a POPC lipid membrane is in a liquid disordered state at 20 °C (T_m; POPC = -2 °C [49]), cholesterol incorporation strongly increased the GP of POPC membranes at 20 °C resulting in membrane packing more similar to DPPC membranes (Fig. 5c). Likewise, the membrane fluidity of POPC liposomes decreased in the presence of cholesterol, indicated by an increased anisotropy (Fig. 5b). Based on the packing/fluidity results observed for membranes containing only PC lipids, a decrease in lytic activity of MbxA would be in accordance. However, the contrary is observed, as instead, cholesterol increases the lytic activity to levels comparable with DOPC membranes (Fig. 5d). As no such effect was observed for proMbxA, the specific role of the acyl-moieties in the lytic activity of this protein with cholesterol is highlighted once again.

To further specify the impact of cholesterol on membrane fluidity and packing, liposomes containing DOPC:Chol 1:1, and DPPC:Chol 1:1, were tested for anisotropy and GP (Fig. 5e,f) while assessing the lytic activity of MbxA and proMbxA on these formulations (Fig. 5g). In all cases, cholesterol incorporation stimulated the lytic activity of MbxA, although no such increase was observed for proMbxA (Fig. 5g). DOPC lipid membrane is in a liquid disordered state while DPPC membrane is in a gel phase at 20 °C (T_m; DOPC = -17 °C [50], DPPC = 41 °C [51]). Anisotropy measurements showed that cholesterol reduces the fluidity of DOPC liposomes, similar to POPC liposomes, while increasing the fluidity of DPPC liposomes (Fig. 5e). GP values for DOPC:Chol liposomes strongly increased, as observed for POPC:Chol liposomes, while the membrane fluidity of DPPC and DPPC:Chol 1:1 liposomes were similar, possibly caused by saturation of the signal (Fig. 5f). Altogether, these results clearly show the specific impact of cholesterol on the lytic activity of MbxA. Nevertheless, a secondary effect can be attributed to the membrane packing as an increase in GP coincides with reduced lytic activity both in the presence and absence of cholesterol.

Interestingly, while cholesterol incorporation into DOPC liposomes increased membrane packing (as indicated by GP measurements; Fig. 5d) and reduced membrane fluidity (as shown by anisotropy measurements; Fig. 5e) compared to DOPC liposomes, proMbxA was capable of inducing lytic activity toward DOPC:Chol 1:1 liposomes. This finding is in contrast with the results from POPC:Chol 1:1 and DPPC:chol 1:1 liposomes, where MbxA exhibited lytic activity, but proMbxA did not. This result indicates that the positive effect of cholesterol on the lytic activity of MbxA is not entirely dependent on the acyl-moieties of the protein. Previous studies have reported that incorporating cholesterol into DOPC membranes (but not for POPC or DPPC membranes) can lead to phase separation within the membrane [52–54].

2.7. *MbxA is unable to induce cytotoxicity when cholesterol is removed from human epithelial (HEp-2) cells*

Although the above *in vitro* results clearly demonstrate the effect of cholesterol on the activity of MbxA, they hardly represent an *in vivo* membrane. Cellular membranes contain a wide variety of different lipids that vary in headgroup and lipid tail configuration. To investigate the *in vivo* effects of cholesterol on the cytotoxicity of MbxA and proMbxA,

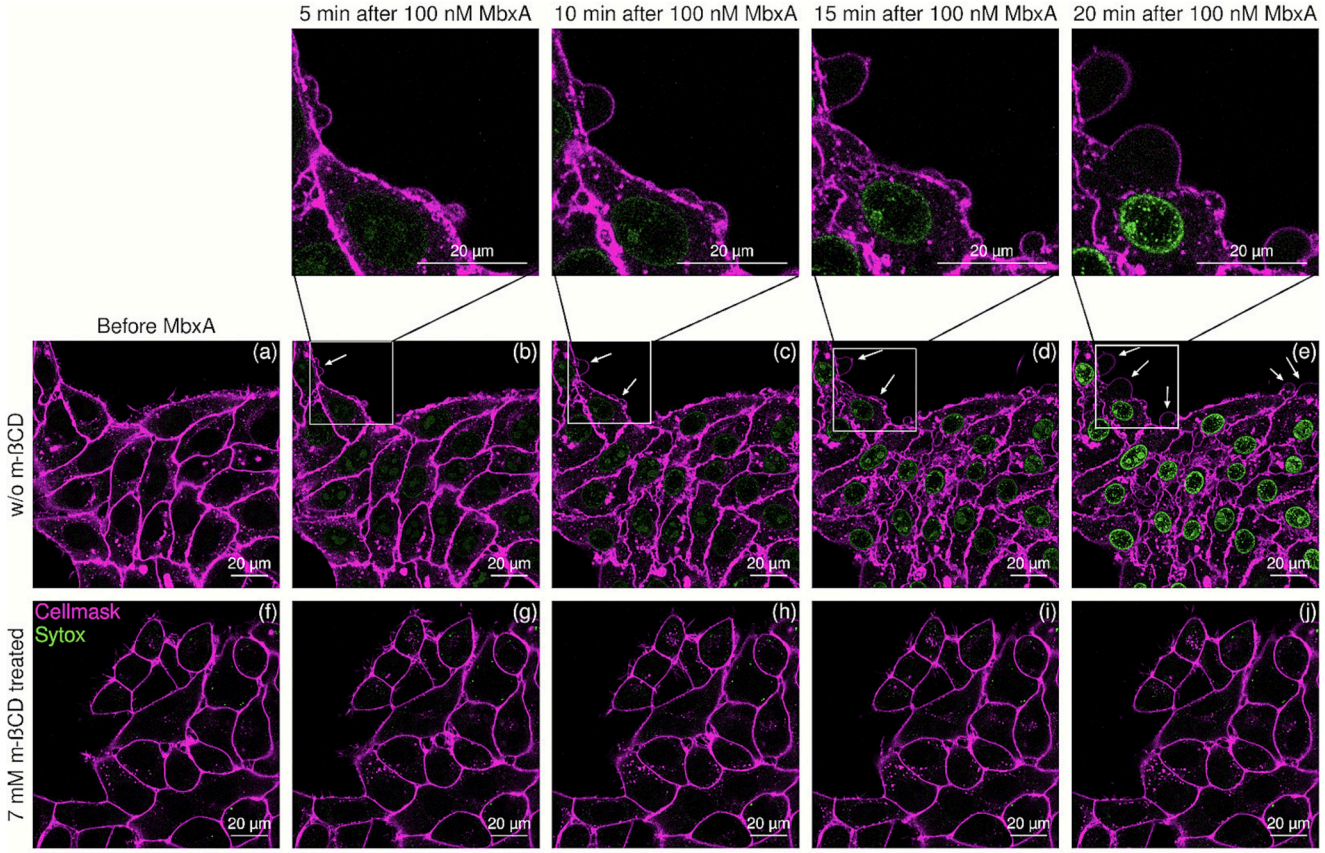

Fig. 6. Confocal microscopy images of CellMask™ Deep Red-stained HEp-2 cells. Second row (a,b,c,d,e): Nuclear staining of HEp-2 cells by Sytox green from the surrounding media due to the plasma membrane permeabilization and membrane blebbing (white arrowheads) resulting from the MbxA cytotoxicity in cholesterol-intact membranes of the HEp-2 cells. The corresponding zoomed-in images of the white insets in b,c,d,e are shown in the first row, where the membrane blebs and Sytox green are visible in more detail. Third row (f,g,h,i,j): No nuclear staining nor membrane blebbing phenotype has been observed in HEp-2 cells when cholesterol-removed HEp-2 cells are incubated with 100 nM MbxA. The data shown are representative of two biological replicates.

their lytic activity was tested on HEp-2 cells with and without cholesterol. HEp-2 cells contain 24.5 % cholesterol [55]. Cytotoxicity was assessed by observing plasma membrane permeabilization and membrane blebbing, which serve as indicators of MbxA-induced cytotoxicity, as described previously [37]. HEp-2 cells were stained with CellMask™ Deep Red to visualize the plasma membrane and suspended in a medium containing Sytox Green, a plasma membrane impermeable nuclear staining dye. Following incubation with MbxA, the plasma membrane of the HEp-2 cells became permeabilized, allowing Sytox Green to stain the nuclei (Fig. 6; first row). Additionally, MbxA cytotoxicity led to a membrane blebbing phenotype, with noticeable blebbing observed just 5 min after MbxA treatment (Fig. 6b, arrowheads). The size of the bleb and intensity of the nuclear staining slowly increases in the subsequent time points, which can be visualized in the 10-min, 15-min, and 20-min images of MbxA treatment on cholesterol-intact HEp-2 cells (Fig. 6; first row). A quantification of time-dependent nuclear staining was performed in the previous work [37]. After 20 min of incubation, more pronounced nuclear staining by Sytox Green and an increase in the number of membrane blebs were evident. Supplementary fig. 3b illustrates a broader area of HEp-2 cells subjected to MbxA, highlighting the Sytox Green permeabilization and membrane blebbing, while supplementary fig. 3c shows the top layer of HEp-2 cells where membrane blebs are prominently visible. To deplete cholesterol, varying concentrations of methyl beta-cyclodextrin (m-βCD) were used, after which the cholesterol content was assessed by GC–MS (Supplementary fig. 3a). As the viability of the cells decreased above 10 mM m-βCD, a concentration of 7 mM was chosen for the experiment. This reduces the total cholesterol content, leaving 2.2–3.9 % of the total content of 24.5 %. When cholesterol was removed from HEp-2 cells using 7 mM m-βCD, MbxA failed to induce cytotoxicity. No nuclear staining by Sytox Green or membrane blebbing was observed, even after 20 min of incubation with 100 nM MbxA (Fig. 6; second row). Notably, whether cholesterol was present or absent, proMbxA did not induce cytotoxicity in HEp-2 cells, consistent with previous observations [37] (Supplementary fig. 3d).

2.8. MbxA & proMbxA bind to HEp-2 cell membranes with and without cholesterol

The flotation assay indicated that both MbxA and proMbxA can associate with POPC:Chol membranes, suggesting that the acyl chains are not required for membrane binding. To validate this finding *in vivo*, both MbxA and proMbxA were labeled with Atto-488, allowing for visualization of their binding to the HEp-2 cell membrane.

HEp-2 cells were treated with 100 nM Atto488-MbxA^{S9C}(Fig. 7b), and any unbound protein was subsequently washed away to highlight the membrane-bound protein (Fig. 7c). As previously reported [37], with a lytic activity of 97 % of the wild-type protein, Atto488-MbxA^{S9C} effectively bound to the plasma membrane of HEp-2 cells (Fig. 7c). To investigate whether cholesterol in the host cell membrane is essential for the binding process of the toxin, Atto 488-labeled MbxA was incubated with cholesterol-removed HEp-2 cells (Fig. 7e) and subsequently washed away (Fig. 7f). Atto488-MbxA^{S9C} was able to bind to the cholesterol-removed plasma membrane of HEp-2 cells, similarly to the binding observed in cholesterol-intact HEp-2 cells (Fig. 7f), indicating that cholesterol is not involved in the initial binding process of the protein to the membrane.

To examine if the acyl chain is necessary for the binding of MbxA to the HEp-2 cell plasma membrane, atto 488-labeled proMbxA was added to both cholesterol-intact (Fig. 7g, h, i) and cholesterol-removed HEp-2 cells (Fig. 7j, k, l). Similar to MbxA, proMbxA was also observed to bind clearly to the plasma membrane of both cholesterol-intact (Fig. 7i) and cholesterol-removed HEp-2 cells (Fig. 7l). This experiment demonstrates that the acyl chain is not necessary for the initial binding of MbxA to the HEp-2 cell membrane.

A control experiment with 100 nM Atto-488 dye showed no binding to the HEp-2 cell membrane, further confirming that the binding of Atto488-MbxA^{S9C} and Atto488-proMbxA^{S9C} is due to the proteins themselves rather than free dye (Sup. Fig. 4). Additionally, a control experiment involving wheat germ agglutinin (WGA) binding to the HEp-2 cell membrane exhibited a binding pattern similar to that of Atto488-MbxA^{S9C} and Atto488-proMbxA^{S9C}, reinforcing the conclusion that these proteins are indeed binding to the plasma membrane of the HEp-2 cells (Sup. Fig. 4). The stability and activity of the labeled proteins were confirmed using an SDS gel and hemoglobin release assay (Sup. Fig. 5).

3. Discussion

RTX toxins, such as MbxA from *M. bovis,* display virulence by disrupting the host cell membranes. Besides the β_2 integrin receptor-dependent activity, RTX toxins can exhibit lytic activity *via* a β_2 integrin receptor-independent interaction pathway, which is suggested to rely on specific interactions between the two acyl-moieties of the RTX toxin with the membrane [4,22,27–36]. Here, we systematically characterized the role of the lipid membrane in the binding and lytic activity of MbxA (acylated at lysine residues K536 and K660 [37]), and its non-acylated counterpart proMbxA.

Introducing negatively charged lipids, exemplified by POPS (Fig. 2b), into neutral liposomes enhances the lytic activity of both MbxA and ProMbxA, illustrating this effect is independent on the acyl-moieties of the protein. This stimulating effect may be explained by a net positive surface charge density of the pore-forming hydrophobic domain at the N-terminus, as indicated by a model of proMbxA predicted by AlphaFold, which was verified by the SAXS (Sup. Fig. 1). Putting this into context, negatively charged lipids are predominantly located in the inner leaflet of host cell membranes and therefore not accessible for RTX toxins [45]. However, during cell signaling or apoptosis, these lipids could be transiently exposed, potentially allowing the toxins to exploit these conditions for binding.

Similarly, introduction of unsaturated acyl chains in the liposomal lipids also increases the lytic activity of MbxA and proMbxA (Fig. 2a). This can be directly linked to changes in the biophysical properties of the membrane *i.e.*, decreased membrane packing and to a lesser extent increased fluidity (Fig. 5b,c), thereby facilitating the membrane its accessibility. Noteworthy, the lytic activity of proMbxA compared to MbxA is severely lower in POPC membranes, possibly highlighting a specific role for the acyl-chain moieties of the protein while interacting with the membrane. Although POPC membranes most closely resemble the acyl-chain configuration of native membranes [45], membrane packing and fluidity are also greatly influenced by sterols. Upon addition of cholesterol, the membrane fluidity decreased, whereas membrane packing drastically increased to levels comparable with DPPC liposomes. Counterintuitively, the incorporation of cholesterol (or ergosterol) into POPC liposomes significantly increased MbxA-induced liposomal leakage, rising from 20 % in POPC liposomes to 45 % in POPC:Chol liposomes (Fig. 2c), which can only be explained by a specific interaction of MbxA with cholesterol. Noteworthy, a (small) decrease in lytic activity was observed for proMbxA, illustrating a particular role for the MbxA acyl-chain moieties in the specific interaction with cholesterol. In other words, the enhanced lytic activity is caused by a specific interaction of acylated MbxA with cholesterol, and not a result of an overall more accessible, less stiff, membrane. A possible explanation for this could be that MbxA accumulates cholesterol into microdomains, thereby creating a favorable local environment for the protein. However, additional experiments would be required to confirm the presence of actual microdomains. To that respect, phase separation has not been reported for POPC:Chol 1:1 liposomes, but is observed in DOPC:Chol 1:1 liposomes, which may explain the observed lytic activity of the non-acylated proMbxA [52–54]. Noteworthy, enhanced lytic activity was observed for ergosterol as well, indicating that this phenomenon could be general for sterols.

Overall, the *in vitro* setup provides a systematic overview, displaying several factors (*e.g.,* lipid charge, membrane packing, sterols, *etc.*) that

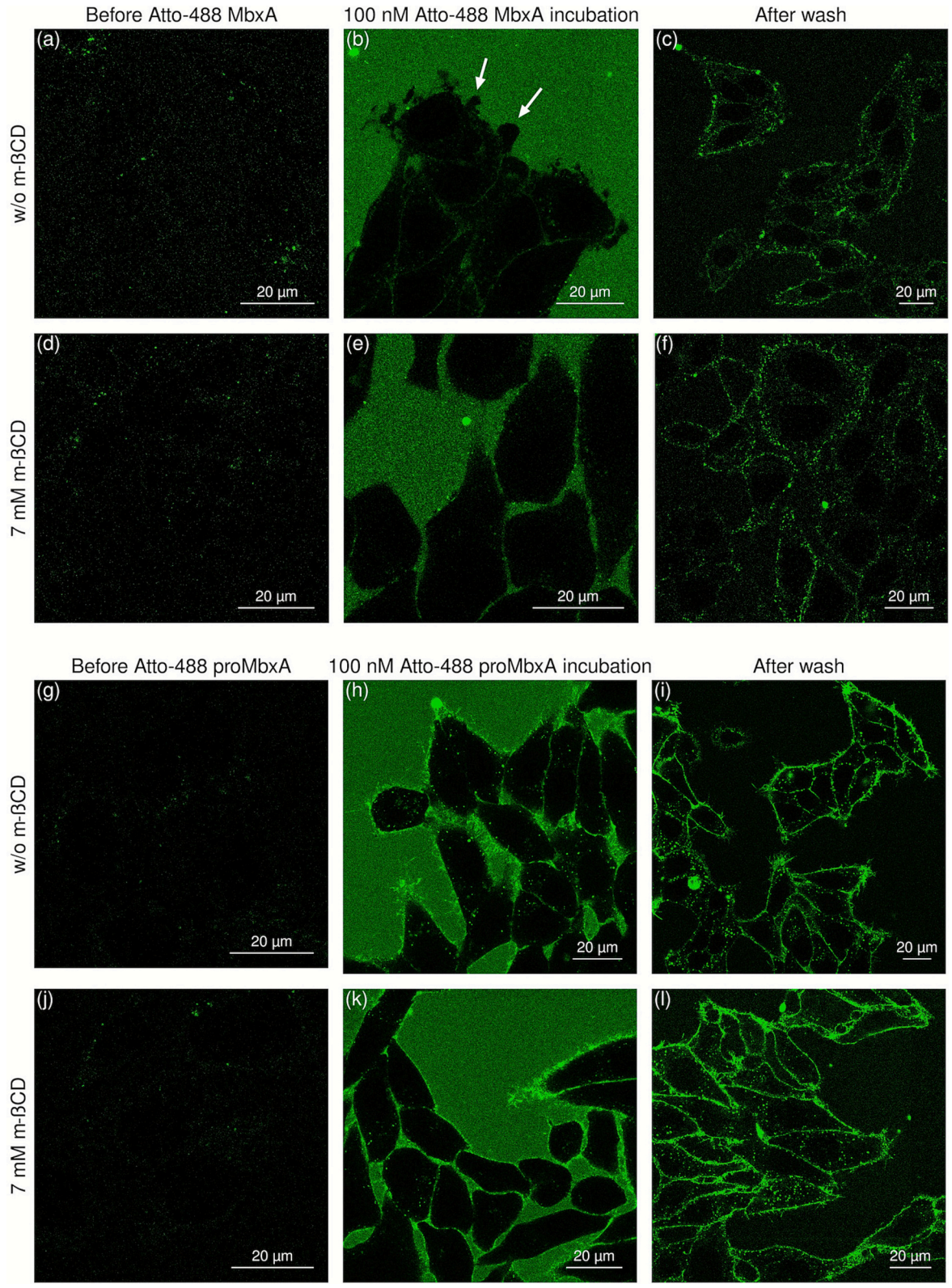

Fig. 7. Confocal microscopy images of (a,b,c) cholesterol intact HEp-2 cells; (a) before incubating with Atto488-MbxA^{S9C}, (b) incubation of HEp-2 cells with Atto488-MbxA^{S9C} which results in membrane blebbing, (c) HEp-2 cells after the excessive unbound protein being washed away. (d,e,f) Cholesterol removed HEp-2 cells using 7 mM m- βCD; (d) before incubating with Atto488-MbxA^{S9C}, (e) incubation of HEp-2 cells with Atto488-MbxA^{S9C} which doesn't show any membrane blebbing, (f) HEp-2 cells after the excessive unbound protein being washed away. (g,h,i) cholesterol intact HEp-2 cells; (g) before incubating with Atto488-proMbxA^{S9C}, (h) incubation of HEp-2 cells with Atto488-proMbxA^{S9C} which doesn't show any membrane blebbing, (i) HEp-2 cells after the excessive unbound protein being washed away. (j,k,l) Cholesterol removed HEp-2 cells using 7 mM m- βCD; (j) before incubating with Atto488-proMbxA^{S9C}, (k) incubation of HEp-2 cells with Atto488-proMbxA^{S9C} which doesn't show any membrane blebbing, (l) HEp-2 cells after the excessive unbound protein being washed away. The data shown are representative of two biological replicates.

play a role in (pro)MbxA activity. Nevertheless, liposomes are simplified model membranes and do not necessarily represent the *in vivo* situation. Using HEp-2 cells as a model system, we tested (pro)MbxA activity in presence and absence of cholesterol. In short, MbxA only showed pore forming activity in normal cholesterol containing membranes, allowing the membrane impermeable Sytox Green to stain the nucleus. On the contrary, depleting the cholesterol content resulted in inactive MbxA. In the case of proMbxA, no lytic activity was observed, regardless of the cholesterol content, thereby confirming the earlier observed difference in the *in vitro* setup. Altogether, the *in vivo* experiments provide critical insights into the combined role of cholesterol and acylation in MbxA's cytotoxic activity within a physiological context. The complete abrogation of lysis in cholesterol-depleted HEp-2 cells underscores its necessity for MbxA's functional conformation and pore formation. This finding aligns with previous studies implicating the presence of cholesterol-rich regions in the activity of pore-forming toxins, further cementing cholesterol as a key lipid component for RTX toxin-mediated cytotoxicity [26,32,36,56,57].

A possible explanation for the cholesterol-dependent lytic activity of MbxA is that the presence of cholesterol results in the formation of more (stable) pores. To determine whether the acyl chains are essential for the binding of MbxA to cholesterol membranes, *in vivo* experiments using confocal microscopy were performed, showing both Atto-488-labeled MbxA^{S9C} and proMbxA^{S9C} were bound to the plasma membrane of HEp-2 cells, regardless of cholesterol presence (Fig. 7). Moreover, an *in vitro* flotation assay with liposomes revealed that after centrifugation both acylated MbxA and non-acylated proMbxA were present in the liposome fraction, although with slightly lower levels of proMbxA. These observations highlight that the initial membrane binding of MbxA is not dependent on its acyl-chains or on cholesterol.

Overall, these results highlight the intricate interplay between lipid composition and protein acylation on the pore-forming behavior of MbxA. However, the specific MbxA- membrane/cholesterol interactions at the molecular level remain unknown. To integrate our experimental results, we propose a model (Fig. 8) illustrating the differential behavior of acylated MbxA and non-acylated proMbxA on cholesterol-containing membranes:

1. Acylation-Induced Conformational Changes: Upon interaction with the membrane, the acyl chains of MbxA may trigger conformational changes that expose specific cholesterol-binding motifs within the protein. Subsequently, cholesterol assists in deeper penetration, possibly stabilizing membrane interactions or stimulating oligomerization of MbxA, thereby promoting pore formation within the membrane. Sequence analysis of MbxA reveals the presence of 25 cholesterol specific CRAC/CARC motifs [60]. In fact, various other RTX proteins are known to possess these specific cholesterol recognition motifs, of which some are located within, or near, the pore-forming domain and found to directly interact with membrane cholesterol [26,36,56,61].
2. MbxA Targets Cholesterol-Enriched Domains: Cholesterol enrichment in specific membrane regions (either pre-existing or induced by MbxA binding) creates a favorable environment that enhances conformational changes, clustering, and/or deep insertion into the bilayer of acylated-MbxA, ultimately resulting in a functional pore. The acyl chains of MbxA might also interact directly with cholesterol, aiding in the stabilization and clustering of the protein within cholesterol-enriched microdomains [28,58,59].

In both scenarios, the acyl chains of MbxA play a critical role toward pore formation. In contrast, proMbxA, lacking these acyl additives, cannot achieve the necessary membrane insertion depth or stability, and therefore remains functionally inactive despite its ability to bind the membrane surface. Our model is consistent with previous observations on the homolog HlyA, where acylated HlyA showed cholesterol-dependent oligomerization in membranes while proHlyA did not [32]. That said, the precise molecular details, such as the role of the cholesterol-binding motifs (*e.g.*, CRAC/CARC sequences), the oligomeric state of active MbxA, and the exact sequence of conformational changes, remain to be determined through structural and computational approaches.

In summary, our *in vitro* and *in vivo* studies elucidate the complex relationships between lipid composition, acylation, and the pore-forming mechanisms of MbxA. The findings highlight cholesterol's essential role in enhancing MbxA's lytic activity facilitated through protein's acylation, even though the acyl chains and cholesterol are not needed for initial membrane binding. The varying effects of different lipid compositions show that secondary factors like membrane fluidity, packing, and surface charge also impact MbxA's function, further emphasizing the complex interplay between protein and membrane. The specific interactions at the molecular level between acylated MbxA and cholesterol remain unknown, but could involve conformational changes that promote pore formation, possibly by activating cholesterol recognition motifs such as CRAC/CARC. The recognition of alternative sterols, like ergosterol, suggests some flexibility of MbxA in adapting to different lipid environments, thereby expanding its range of targets. Overall, these findings deepen our understanding of the molecular factors underlying RTX toxin activity and their role in membrane disruption and cytotoxicity.

4. Materials and methods

4.1. Protein expression & purification

Expression, secretion, and purification of (pro)MbxA were performed as described before [37]. (pro)MbxA was expressed in BL21 (DE3) *E. coli* strains. The proteins were expressed in a two-plasmid system in which one plasmid carries the ABC transporter *hlyBD* gene, and the second carries either the *hlyC-mbxA gene* (for acylated MbxA) or *mbxA* gene (for proMbxA). The expressed proteins were secreted *via* HlyBD, culture supernatants were pooled, and purified by Immobilised Metal Affinity Chromatography (IMAC).

4.2. Hemoglobin release assay

Assays were performed as previously reported [37]. Defibrinated sheep blood cells were washed and centrifuged several times using buffer A until the supernatant became clear. Homogenized blood cells were incubated with 30 nM of protein (MbxA, Atto488-MbxA^{S9C}, proMbxA, Atto488-proMbxA^{S9C}) for 30 min at 37 °C. 16 % SDS and IMAC buffer were used as positive (100 %) and negative (0 %) controls. Cells were then centrifuged, supernatants analyzed for hemoglobin release, and quantified *via* OD on a FLUOstar OPTIMA microplate reader (BMG Labtech) at 544 nm. Buffer A: 10 mM Tris–HCl pH 7.5, 155 mM NaCl, 20 mM CaCl2, 5 mM KCl, and 2 mM MgSO4.

4.3. Liposome preparation and leakage assay

Chloroform-dissolved lipids were dried in a rotary evaporator at 40 °C for 30 min. Lipids were resuspended in 1 ml ANTS buffer (12.5 mM ANTS, 45 mM DPX, 150 mM NaCl, 20 mM Tris-HCl pH 7.0). Lipid suspension was sonicated in six cycles (15 s on/45 s off), 50 % duty cycle, and 50 % (power) at RT. The resulting small unilamellar vesicles (SUVs) were flash-frozen in liquid nitrogen and thawed at room temperature (~20 min) two times. Liposomes were extruded using a 100 nm membrane pore (Extruder: LiposoFast-Basic & Stabilizer, Avestin Inc.), and the liposome size was further confirmed using DLS measurement. Untrapped ANTS+DPX were chromatographically removed through a sephedex G-50 column using 150 mM NaCl, and 20 mM Tris-HCl pH 7.0 (buffer B). The final lipid concentration of 12 uM was calculated based on the dilutions from each step. The liposome leakage experiment was performed in buffer B.

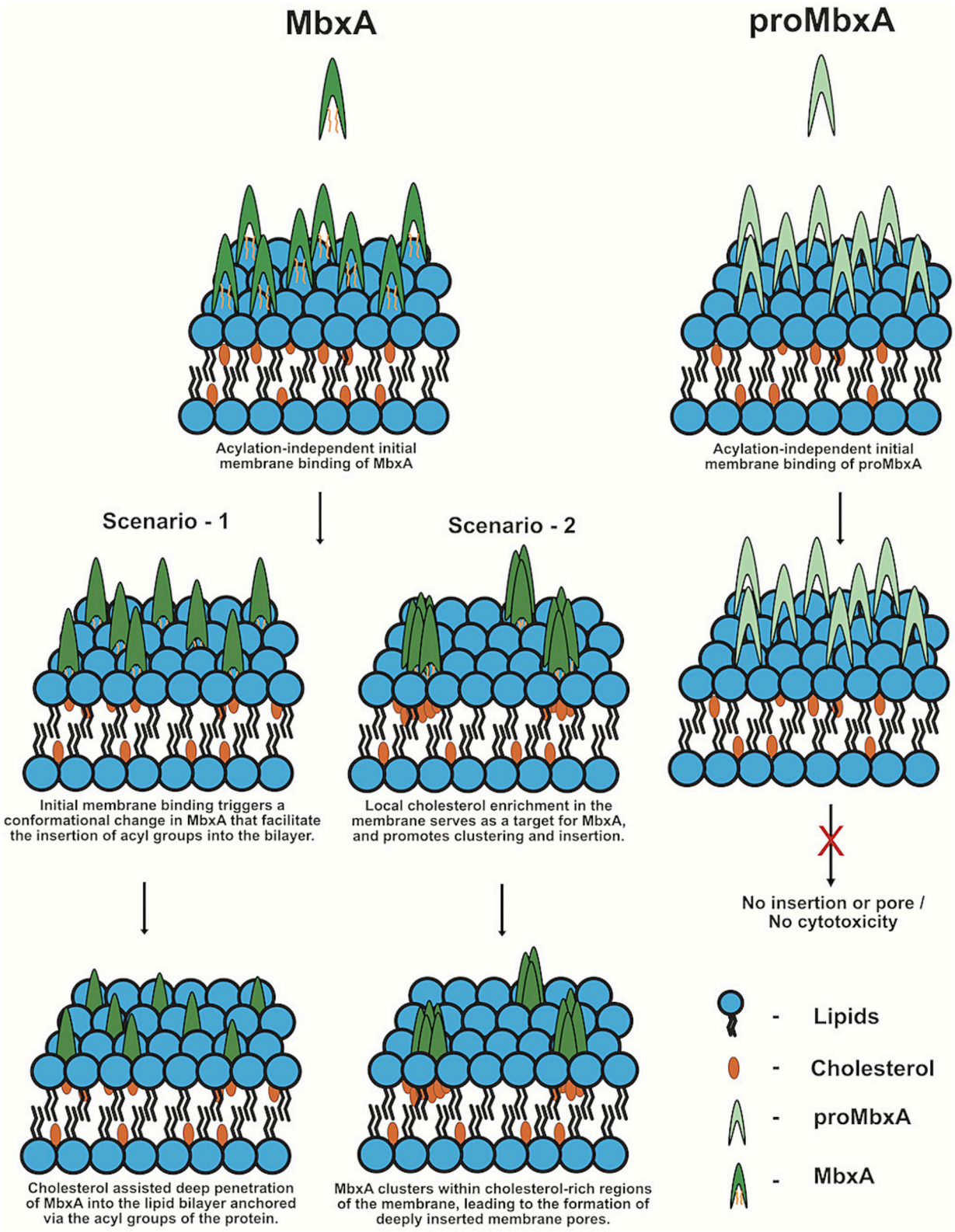

Fig. 8. Proposed membrane interaction model of acylated MbxA versus non-acylated proMbxA in cholesterol-containing membranes. Both MbxA (acylated) and proMbxA (non-acylated) initially bind to cholesterol-containing membranes in an acylation-independent manner (top panel). ProMbxA (right panel), despite initial membrane binding, exerts no toxicity, possibly due to incomplete insertion and/or failed pore formation. On the contrary, MbxA shows toxicity, for which we propose 2 scenarios. (Scenario 1) Upon initial membrane binding, the MbxA acyl chains triggers a conformational change in MbxA that facilitates a cholesterol-assisted deep penetration of MbxA into the lipid bilayer. (Scenario 2) Local cholesterol enrichment serves as a target for MbxA (acylated), promoting clustering and/or deep membrane insertion of the protein.

4.4. GUV preparation and assay

Two indium tin oxide (ITO)-coated glass slides were cleaned with 70 % ethanol and chloroform. Then lipid solution (2*10 μl) was spread on the ITO-coated side, and the lipid area of one slide was fenced by a ring of sigillum wax (Vitrex$_{TM}$). A chamber was prepared by pressing the ITO/lipid-coated sides to each other. The chamber was filled with 300 μl of 10 % sucrose solution and sealed. Incubated the chamber for 3 h at RT, applying an alternating current with 11 Hz and 2 V. GUVs were harvested using a GELoader® tip (Eppendorf). The chamber was incubated with BSA (1 min) before adding GUVs to the observation chamber. The chamber was washed 3 times with PBS. Next, 250 μl PBS + 50 μl GUVs were added to the chamber. 100 nM of (pro)MbxA was added, and time-lapse images were captured for 30 min with 30s time interval.

4.5. Membrane lipid packing and membrane fluidity analysis

Membrane lipid packing was analyzed by measuring General Polarization (GP) and membrane fluidity was analyzed by Anisotropy, by using a Horiba Fluorolog-3 fluorometer. 100 μM SUVs (see liposome preparation section) were mixed with 0.3 μM laurdan to achieve a dye: lipid ratio of 1:333. Samples were incubated at 37 °C for 1 h in the dark, shaking at 300 rpm.

4.5.1. GP measurement

Emission spectra (400-600 nm) were measured while exciting at 350 nm (Entrance slit: 3.00 nm Bandpass; Exit slit: 3.00 nm Bandpass). GP calculation:

$$(I_{435} - I_{500})/(I_{435} + I_{500})$$

where I is fluorescence intensity.

4.5.2. Anisotropy measurement

Single point anisotropy measurement was performed by excitation at 350 nm and an emission monitoring at 435 nm. Anisotropy calculation:

$$r = (I_{vv} - GI_{vh})/(I_{vv} + 2GI_{vh})$$

where I is fluorescence intensity; v (vertical), h (horizontal) settings for the excitation/emission polarizers respectively; G is the instrumental correction factor provided by the instrument.

4.6. Flotation assay

SUVs (see liposome preparation section) were mixed with protein to a final volume of 100 μl and incubated for 5 min at RT. 100 μl 60 % sucrose solution was added, resulting in 30 % sucrose solution with protein and liposomes. The mix was transferred into ultracentrifuge tubes of the AT3 rotor. 250 μl of 20 % sucrose solution was carefully added on top without disturbing the bottom layer. 50 μlL of liposome buffer was added on top and centrifuged at 80,000 rpm for 1 h at 4 °C. After ultracentrifugation, samples were carefully taken from the three layers using a gel loading tip like follows: (1) 250 μlL - Bottom layer (2) 125 μl - Middle layer (3) 125 μl - Top layer. The same volume of 30 % TCA (Trichloroacetic acid) was added to the three fractions. After incubation on ice (15 min), samples were centrifuged (17,000 ×*g*; 15 min; 4 °C) and supernatant TCA removed. 500 μl of ice-cold acetone was added to the pellet, resuspended, incubated on ice (15 min) and centrifuged (17,000 ×*g*; 15 min; 4 °C). Supernatant acetone was removed, pellet dried using a speed vacuum centrifuge (10 min). Pellet was resuspended in 30 μl and analyzed by SDS PAGE.

4.7. Cell culture and live-cell imaging

HEp-2 cells were cultivated and passaged in DMEM (Pan Biotech) supplemented with 10 % FCS, MEM vitamins, non-essential amino acids, amphotericin B (2.5μg/ml), and gentamicin (50μg/ml). Two days before, HEp-2 cells were seeded in 2 ml DMEM in 35 mm μ-Dish 1.5H glass bottom dishes (Ibidi) and grown for 39–48 h at 37 °C under 5 % CO_2. Live-cell DMEM medium with 25 mM HEPES in addition to the above-mentioned components is used for all the subsequent steps. Cells were washed with prewarmed DMEM live-cell medium and cell membranes stained using 5 μg/ml CellMask Deep Red in DMEM-SG (containing 5 μM Sytox Green), for 8 min at 37 °C and 5 % CO_2. Cells were washed with DMEM and replaced with 1 ml DMEM-SG. Images were acquired with Zeiss LSM880 Airyscan. 1 ml DMEM-SG and 200 nM protein was added into 1 ml HEp-2 cells (100 nM final). Images were captured every 5 min after incubation and activity was monitored as described before [37].

Atto488-labeled (pro)MbxA^{S9C} was used to visualize HEp-2 cell membrane binding. HEp-2 cells were washed with DMEM medium, replaced with 1 ml of fresh DMEM medium, and imaged (Zeiss LSM880 Airyscan). Tile-scan images of 1 ml HEp-2 cells were acquired prior to labeled (pro)MbxA and after 10 min incubation (100 nM final) Unbound labeled proteins were washed off using DMEM and replaced with 1 ml of fresh DMEM medium before image acquisition.

4.7.1. Microscopy settings

Confocal and Airyscan micrographs were recorded using a Zeiss LSM880 Airyscan microscope system (Carl Zeiss Microscopy GmbH) equipped with a Plan-Apochromat 63×/1.4 oil immersion objective lens. For excitation, a 405 nm Laser was used for Hoechst 33342, a 488 nm Argon laser for excitation of Sytox Green and Atto488-labeled MbxA^{S9C,} and a 633 nm laser for excitation of CellMask Deep Red.

4.8. Mass spectrometry analysis of cholesterol removal

Cholesterol was removed from HEp-2 cells by incubation with m-βCD 5 mM, 7 mM, 10 mM, 15 mM, or 20 mM (1 h, 5 % CO_2). Prior to GC–MS analysis, 0.5 nanomol (nmol) of internal standard β-sitosterol was added. Lipids were extracted with 0.3 ml n-butanol (2 times), solvent evaporated with nitrogen gas. Dried lipid films were resuspended in 100ul MSTFA and incubated (80 °C; 30 min).

1 μl of derivatized compounds was injected and measured on a 5977B GC/MSD (Agilent Technologies) as described [62]. Oven temperature gradient: constant at 70 °C for 1 min, ramped at 42 °C min^{-1} to 280 °C, further with 4 °C min^{-1} to 320 °C, held constant for 3 min (total 19 min). Electron ionization source: 70 eV; source temperature: 200 °C, mass range: 60-600 *m/z*, 5 scans per second. Metabolites were identified *via* MassHunter Qualitative (v b08.00, Agilent Technologies) by NIST14 Mass Spectral Library comparison (https://www.nist.gov/srd/nist-standard-reference-database-1a-v14). Authentic chemical standards for cholesterol were measured at a concentration of 5,10,50, 100 μM and processed in parallel. Peaks were integrated using MassHunter Quantitative (v b08.00, Agilent Technologies). All metabolite peak areas were normalized to the sample amount (24 K HEp-2 cells) and internal standard β-sitosterol (Sigma-Aldrich).

CRediT authorship contribution statement

Feby Mariam Chacko: Writing – review & editing, Writing – original draft, Investigation, Formal analysis, Data curation. **Sarah Michelle Ganz:** Formal analysis, Data curation. **Anne Pfitzer-Bilsing:** Formal analysis, Data curation. **Sebastian Hänsch:** Writing – review & editing, Supervision, Methodology, Investigation. **Philipp Westhoff:** Writing – review & editing, Investigation. **Stefanie Weidtkamp-Peters:** Writing – review & editing, Methodology, Formal analysis. **Sander H.J. Smits:** Writing – review & editing, Supervision. **Marten Exterkate:** Writing – review & editing, Writing – original draft, Validation, Formal analysis, Data curation. **Lutz Schmitt:** Writing – review & editing, Project administration, Funding acquisition, Conceptualization.

Funding sources

The CEPLAS Plant Metabolism and Metabolomics Laboratory, which is funded by the DFG under Germany's Excellence Strategy—EXC-2048/1—project ID 390686111 (to P.W.). Research was funded by the Jürgen Manchot Foundation through a project in the Manchot graduate school 'Molecules of Infections IV' to L.S.

Declaration of competing interest

The authors declare that they have no known competing financial interests or personal relationships that could have appeared to influence the work reported in this paper.

Acknowledgments

We thank all members of the Institute of Biochemistry for fruitful and stimulating discussions. We are thankful for excellent technical support from Elisabeth Klemp.

Appendix A. Supplementary data

Supplementary data to this article can be found online at https://doi.org/10.1016/j.bbamem.2025.184487.

Data availability

Data will be made available on request.

References

[1] I.B. Holland, et al., Type I protein secretion—deceptively simple yet with a wide range of mechanistic variability across the family, EcoSal Plus 7 (1) (2016), p. 10.1128/ecosalplus. ESP-0019-2015.
[2] R. Benz, et al., Pore formation by the Escherichia coli hemolysin: evidence for an association-dissociation equilibrium of the pore-forming aggregates, Infect. Immun. 57 (3) (1989) 887–895.
[3] L.C. Ristow, et al., The extracellular domain of the β(2) integrin β subunit (CD18) is sufficient for *Escherichia coli* Hemolysin and Aggregatibacter actinomycetemcomitans Leukotoxin cytotoxic activity, mBio 10 (4) (2019).
[4] J. Vojtova, J. Kamanova, P. Sebo, Bordetella adenylate cyclase toxin: a swift saboteur of host defense, Curr. Opin. Microbiol. 9 (1) (2006) 69–75.
[5] A.C. Brown, et al., Membrane localization of the repeats-in-toxin (RTX) Leukotoxin (LtxA) produced by Aggregatibacter actinomycetemcomitans, PLoS One 13 (10) (2018) e0205871.
[6] F.M. Chacko, L. Schmitt, Interaction of RTX toxins with the host cell plasma membrane, Biol. Chem. 404 (7) (2023) 663–671.
[7] P.J. Bakkes, et al., The rate of folding dictates substrate secretion by the Escherichia coli hemolysin type 1 secretion system, J. Biol. Chem. 285 (52) (2010) 40573–40580.
[8] V. Koronakis, et al., Crystal structure of the bacterial membrane protein TolC central to multidrug efflux and protein export, Nature 405 (6789) (2000) 914–919.
[9] J.-M. Nicaud, et al., Characterisation of HlyC and mechanism of activation and secretion of haemolysin from E. coli 2001, FEBS Lett. 187 (2) (1985) 339–344.
[10] I.B. Holland, L. Schmitt, J. Young, Type 1 protein secretion in bacteria, the ABC-transporter dependent pathway, Mol. Membr. Biol. 22 (1–2) (2005) 29–39.
[11] I. Linhartová, et al., RTX proteins: a highly diverse family secreted by a common mechanism, FEMS Microbiol. Rev. 34 (6) (2010) 1076–1112.
[12] R.P. Dassanayake, S.K. Maheswaran, S. Srikumaran, Monomeric expression of bovine beta2-integrin subunits reveals their role in Mannheimia haemolytica leukotoxin-induced biological effects, Infect. Immun. 75 (10) (2007) 5004–5010.
[13] T. Dileepan, et al., Human CD18 is the functional receptor for Aggregatibacter actinomycetemcomitans leukotoxin, Infect. Immun. 75 (10) (2007) 4851–4856.
[14] J.A. Goldsmith, et al., Structural basis for non-canonical integrin engagement by Bordetella adenylate cyclase toxin, Cell Rep. 40 (7) (2022) 111196.
[15] P. Guermonprez, et al., The adenylate cyclase toxin of Bordetella pertussis binds to target cells via the alpha(M)beta(2) integrin (CD11b/CD18), J. Exp. Med. 193 (9) (2001) 1035–1044.
[16] S. Jeyaseelan, et al., Lymphocyte function-associated antigen 1 is a receptor for Pasteurella haemolytica leukotoxin in bovine leukocytes, Infect. Immun. 68 (1) (2000) 72–79.
[17] E.T. Lally, et al., RTX toxins recognize a β2 integrin on the surface of human target cells, J. Biol. Chem. 272 (48) (1997) 30463–30469.
[18] J. Li, K.D. Clinkenbeard, J.W. Ritchey, Bovine CD18 identified as a species specific receptor for *Pasteurella haemolytica* leukotoxin, Vet. Microbiol. 67 (2) (1999) 91–97.
[19] J. Reinholdt, et al., Monodisperse and LPS-free Aggregatibacter actinomycetemcomitans leukotoxin: interactions with human β2 integrins and erythrocytes, Biochim. Biophys. Acta 1834 (2) (2013) 546–558.
[20] P.G. Vanden Bergh, et al., Porcine CD18 mediates Actinobacillus pleuropneumoniae ApxIII species-specific toxicity, Vet. Res. 40 (4) (2009) 33.
[21] J.F. Wang, et al., Molecular and biochemical mechanisms of Pasteurella haemolytica leukotoxin-induced cell death, Microb. Pathog. 25 (6) (1998) 317–331.
[22] W.U. Rahman, et al., Binding of Kingella kingae RtxA toxin depends on cell surface oligosaccharides, but not on β(2) Integrins, Int. J. Mol. Sci. 21 (23) (2020).
[23] N.V. Balashova, et al., Leukotoxin confers beta-hemolytic activity to Actinobacillus actinomycetemcomitans, Infect. Immun. 74 (4) (2006) 2015–2021.
[24] A. Valeva, et al., Binding of Escherichia coli hemolysin and activation of the target cells is not receptor-dependent, J. Biol. Chem. 280 (44) (2005) 36657–36663.
[25] C. Martín, et al., Membrane restructuring by Bordetella pertussis adenylate cyclase toxin, a member of the RTX toxin family, J. Bacteriol. 186 (12) (2004) 3760–3765.
[26] A. Osickova, et al., Cytotoxic activity of Kingella kingae RtxA toxin depends on post-translational acylation of lysine residues and cholesterol binding, Emerg Microbes Infect 7 (1) (2018) 178.
[27] A.L. Cortajarena, F.M. Goñi, H. Ostolaza, Glycophorin as a receptor for *Escherichia coli* alpha-hemolysin in erythrocytes, J. Biol. Chem. 276 (16) (2001) 12513–12519.
[28] K.P. Fong, et al., Actinobacillus actinomycetemcomitans leukotoxin requires lipid microdomains for target cell cytotoxicity, Cell. Microbiol. 8 (11) (2006) 1753–1767.
[29] M.S. Forman, et al., Gangliosides block Aggregatibacter Actinomycetemcomitans leukotoxin (LtxA)-mediated hemolysis, Toxins (Basel) 2 (12) (2010) 2824–2836.
[30] Intoxication of human phagocytes by bordetella adenylate-cyclase toxin-implication of a ganglioside receptor, in: P. Gable, J. Eaton, D. Confer (Eds.), Clinical Research, Slack Inc, 6900 Grove Rd, Thorofare, NJ 08086, 1985.
[31] V.M. Gordon, et al., Adenylate cyclase toxins from Bacillus anthracis and Bordetella pertussis. Different processes for interaction with and entry into target cells, J. Biol. Chem. 264 (25) (1989) 14792–14796.
[32] V. Herlax, et al., Relevance of fatty acid covalently bound to Escherichia coli alpha-hemolysin and membrane microdomains in the oligomerization process, J. Biol. Chem. 284 (37) (2009) 25199–25210.
[33] J. Morova, et al., RTX cytotoxins recognize beta2 integrin receptors through N-linked oligosaccharides, Proc. Natl. Acad. Sci. USA 105 (14) (2008) 5355–5360.
[34] L. Mrówczyńska, et al., Bordetella adenylate cyclase toxin can bind Ganglioside GM1, BIO 1 (2011) 67–71.
[35] P.S. Munksgaard, et al., Sialic acid residues are essential for cell lysis mediated by leukotoxin from Aggregatibacter actinomycetemcomitans, Infect. Immun. 82 (6) (2014) 2219–2228.
[36] R.F. Vazquez, et al., Novel evidence for the specific interaction between cholesterol and α-haemolysin of Escherichia coli, Biochem. J. 458 (3) (2014) 481–489.
[37] I.N. Erenburg, et al., Heterologously secreted MbxA from Moraxella bovis induces a membrane blebbing response of the human host cell, Sci. Rep. 12 (1) (2022) 17825.
[38] J.A. Angelos, J.F. Hess, L.W. George, Cloning and characterization of a Moraxella bovis cytotoxin gene, Am. J. Vet. Res. 62 (8) (2001) 1222–1228.
[39] J.A. Angelos, J.F. Hess, L.W. George, An RTX operon in hemolytic Moraxella bovis is absent from nonhemolytic strains, Vet. Microbiol. 92 (4) (2003) 363–377.
[40] P.J. Baptista, Infectious bovine keratoconjunctivitis: a review, Br. Vet. J. 135 (3) (1979) 225–242.
[41] M.K. Beard, L.J. Moore, Reproduction of bovine keratoconjunctivitis with a purified haemolytic and cytotoxic fraction of Moraxella bovis, Vet. Microbiol. 42 (1) (1994) 15–33.
[42] K.D. Clinkenbeard, A.E. Thiessen, Mechanism of action of Moraxella bovis hemolysin, Infect. Immun. 59 (3) (1991) 1148–1152.
[43] J.B. Henson, L.C. Grumbles, Infectious bovine Keratoconjunctivitis. 1. Etiology, Am. J. Vet. Res. 21 (84) (1960) 761–766.
[44] J.F. Hess, J.A. Angelos, The Moraxella bovis RTX toxin locus mbx defines a pathogenicity island, J. Med. Microbiol. 55 (Pt 4) (2006) 443–449.
[45] J. Lorent, et al., Plasma membranes are asymmetric in lipid unsaturation, packing and protein shape, Nat. Chem. Biol. 16 (6) (2020) 644–652.
[46] F.M. Harris, K.B. Best, J.D. Bell, Use of laurdan fluorescence intensity and polarization to distinguish between changes in membrane fluidity and phospholipid order, Biochim. Biophys. Acta 1565 (1) (2002) 123–128.
[47] S.A. Sánchez, et al., Laurdan generalized polarization: from cuvette to microscope. Modern research and educational topics in microscopy 2 (2007) 1007–1014.
[48] M. Kamel, et al., Unsaturated fatty acids augment protein transport via the SecA: SecYEG translocon, FEBS J. 289 (1) (2022) 140–162.
[49] U. Wanderlingh, et al., Molecular dynamics of POPC phospholipid bilayers through the gel to fluid phase transition: an incoherent quasi-elastic neutron scattering study, J. Chem. 2017 (1) (2017), p. 3654237.
[50] A.S. Ulrich, M. Sami, A. Watts, Hydration of DOPC bilayers by differential scanning calorimetry, Biochim. Biophys. Acta 1191 (1) (1994) 225–230.
[51] R.L. Biltonen, D. Lichtenberg, The use of differential scanning calorimetry as a tool to characterize liposome preparations, Chem. Phys. Lipids 64 (1–3) (1993) 129–142.
[52] T. Baumgart, S.T. Hess, W.W. Webb, Imaging coexisting fluid domains in biomembrane models coupling curvature and line tension, Nature 425 (6960) (2003) 821–824.
[53] R.-X. Gu, S. Baoukina, D.P. Tieleman, Phase separation in atomistic simulations of model membranes, J. Am. Chem. Soc. 142 (6) (2020) 2844–2856.

[54] N.T. Matsuki, Masaki Goto, Hitoshi, Phase separation in phospholipid bilayers induced by cholesterol, in: Encyclopedia of Biocolloid and Biointerface Science 2V Set, 2016, pp. 825–840.
[55] R.T. Coones, R. Green, R. Frazier, Investigating lipid headgroup composition within epithelial membranes: a systematic review, Soft Matter 17 (28) (2021) 6773–6786.
[56] A.C. Brown, et al., Aggregatibacter actinomycetemcomitans leukotoxin utilizes a cholesterol recognition/amino acid consensus site for membrane association, J. Biol. Chem. 288 (32) (2013) 23607–23621.
[57] D. González Bullón, et al., Cholesterol stimulates the lytic activity of adenylate cyclase toxin on lipid membranes by promoting toxin oligomerization and formation of pores with a greater effective size, FEBS J. 288 (23) (2021) 6795–6814.
[58] D.N. Atapattu, C.J. Czuprynski, Mannheimia haemolytica leukotoxin binds to lipid rafts in bovine lymphoblastoid cells and is internalized in a dynamin-2-and clathrin-dependent manner, Infect. Immun. 75 (10) (2007) 4719–4727.
[59] L. Bumba, et al., Bordetella adenylate cyclase toxin mobilizes its β2 integrin receptor into lipid rafts to accomplish translocation across target cell membrane in two steps, PLoS Pathog. 6 (5) (2010) e1000901.
[60] I. Erenburg, Functional and structural characterization of the RTX proteins MbxA from Moraxella bovis and FrpA from *Kingella kingae*, in: Dissertation, Heinrich-Heine-Universität, Düsseldorf, 2020.
[61] H. Ostolaza, J. Amuategi, Membrane interaction characteristics of the RTX toxins and the cholesterol-dependence of their cytolytic/cytotoxic activity, Int. J. Mol. Sci. 25 (6) (2024) 3131.
[62] S.-H. Shim, et al., Loss of function of rice plastidic glycolate/glycerate translocator 1 impairs photorespiration and plant growth, Front. Plant Sci. 10 (2020) 1726.